Oxidative Degradation of a Sulfonamide-Containing 5,6-Dihydro-4-Hydroxy-2-Pyrone in Aqueous/Organic Cosolvent Mixtures

Susan W. Hovorka,[1] Michael J. Hageman,[2] and Christian Schöneich[1,3]

Received December 17, 2001; accepted January 4, 2002

Purpose. To predict the oxidative stability of a sulfonamide-containing 5,6-dihydro-4-hydroxy-2-pyrone in lipid-based delivery systems, *N*-(3-{1[(3α,6R)-4-hydroxy-2-oxo-6-phenyl-6-propyltetrahydro-2H-pyran-3-yl]propyl}phenyl)-5-(trifluoromethyl)-2-pyridinylsulfonamide (DHP) was oxidized by peroxides and peroxyl radicals in binary mixtures of water and organic cosolvents.

Methods. DHP was oxidized by hydrogen peroxide, t-butylhydroperoxide, or peroxyl radicals derived from the thermal decomposition of 2,2′-azobis(2-amidinopropane) dihydrochloride (AAPH) in 40% (v/v) organic cosolvent and 5 mM buffer at or near 40°C. Interactions between DHP and]propane sulfonic acid and imidazole) and DH^- were assessed by ^{1}H-NMR spectroscopy. The formation of CO likely involves a free radical mechanism.

Results. The reaction of DHP with peroxides in 40% (v/v) acetonitrile yields epimeric monohydroxylation products, R-OH and S-OH, at C-3 of the pyrone ring, and a keto-derivative (CO). Hydroxylation rates depend on the protonation state of DHP, and the nature of buffer and the organic cosolvent. Organonitriles accelerate the oxidation through formation of peroxycarboximidic acid. Peroxyl radicals do not yield significant amounts of R/S-OH or CO.

Conclusions. The hydrogen peroxide-induced degradation of DHP in the presence of acetonitrile involves two reactions, hydroxylation and carbonyl formatin. Hydroxylation proceeds via nucleophilic attack by the monodeprotonated form of DHP (DH^-) on peroxycarboximidic acid. The oxidation rate is slowed by ion pairing between nitrogen-containing buffers ([3-*N*-morpholino]propane sulfonic acid and imidazole) and DH^-. The formation of CO likely involves a free radical mechanism.

KEY WORDS: 5,6-dihydro-4-hydroxy-2-pyrone; stability; oxidation; hydroxylation; peroxycarboximidic acid; Payne oxidation.

INTRODUCTION

In the mid-1990s specific antiviral activities were reported for warfarin-based molecules, such as 4-hydroxypyran-2-ones (1–3), 4-hydroxy-2-pyrones (1,4) and 5,6-dihydro-4-hydroxy-2-pyrones (5–7). Structure–activity-based design has identified a sulfonamide-containing derivative with a chiral center positioned at C6 of the dihydropyrone, *N*-(3-{1-[(3α,6R)-4-hydroxy-2-oxo-6-phenyl-6-propyltetrahydro-2*H*-pyran-3-yl]propyl}phenyl)-5-(trifluoromethyl)-2-pyridinylsulfonamide (DHP) (Fig. 1), as an especially potent and efficacious drug candidate (5,8). DHP has a low intrinsic solubility, estimated at 0.1 μg/mL (8) and has two ionizable sites, the 4-hydroxy group of the dihydropyrone ($pK_{a,1}$ = 5.4) (8) and the sulfonamide group ($pK_{a,2}$ = 8.1) (8). The fully protonated and monodeprotonated forms of the drug, DH_2 and DH^-, respectively, tautomerize between the enol/enolate and diketo/carbanion forms.

As with many hydrophobic drugs, lipid-based delivery systems accommodate hydrophobicity and appropriate drug loads. However, some components of such systems (i.e., surfactants, lipids, and organic cosolvents) are prone to autoxidation [e.g., lipids, for a review on lipid peroxidation see Porter (9)], and such reactions may trigger oxidative reactions of drugs as well. Weak C-H bonds, such as the C-H bond α to C3 in DHP, are the targets of hydrogen abstraction, a common propagation step of autoxidation. The complexity of these systems compromises any detailed elucidation of mechanisms leading to oxidative drug degradation. To obtain meaningful information that is relative to the physical and chemical parameters affecting drug degradation, mechanistic investigations and accelerated stability studies must be performed in simple binary aqueous-organic cosolvent systems, which ensure drug solubility. For example, accelerated stability systems for drugs, such as DHP, are commonly performed in aqueous acetonitrile; however, such aqueous cosolvent mixtures always must be tested carefully with regard to any potential direct effect of the organic cosolvent on drug oxidation.

In the present work, we performed a mechanistic investigation of the oxidative degradation of DHP in binary mixtures of water and organic cosolvents using peroxides [hydrogen peroxide, H_2O_2, and t-butylhydroperoxide, t-buOOH] and peroxyl radicals from 2,2′-azobis(2-amidinopropane) dihydrochloride (AAPH) as oxidants. These two classes of oxidants represent the most prominent oxidizing species that can be expected in potentially autoxidizing lipid formulations. Peroxides can react via homolytic O-O bond cleavage or oxygen transfer reactions. AAPH (R-N=N-R, where R = $-C(CH_3)_2-C(NH)NH_2 \bullet$ HCl) generates peroxyl radicals (ROO•) via Reactions 1 and 2 (10), respectively, which react by H-atom abstraction, addition to alkenes or oxygen transfer (11).

$$R\text{–}N{=}N\text{–}R \xrightarrow{h\nu/\Delta} 2R^\bullet + N_2(g) \quad (1)$$

$$R^\bullet + O_2 \longrightarrow ROO^\bullet \quad (2)$$

EXPERIMENTAL

Materials

DHP was provided by Pharmacia & Upjohn (now Pharmacia; Kalamazoo, MI). Unless specifically stated, chemicals were obtained from Sigma-Aldrich (St. Louis, MO) or Fisher Scientific (Pittsburgh, PA) at the highest commercially available grade. AAPH was purchased from Kodak Fine Chemicals (Rochester, NY). Deuterated solvents and imidazole were purchased from Cambridge Isotope Laboratories (Andover, MA) and Chelex-100 mesh resin from Bio-Rad (Hercules, CA). Water was deionized and filtered with a Water Pro™ PS purification system (Labconco; Kansas City, MO). Positioning rods and ultem susceptibility plugs for use in ^{1}H-

[1] Department of Pharmaceutical Chemistry, The University of Kansas, 2095 Constant Avenue, Lawrence, Kansas 66047.
[2] Pharmacia, Kalamazoo, Michigan 49002.
[3] To whom correspondence should be addressed. (e-mail: schoneic@ukans.edu)

0724-8741/02/0400-0538/0 © 2002 Plenum Publishing Corporation

NMR experiments were purchased from Wilmad Glass (Buena, NJ). Although organic cosolvents were of the highest commercially available grade, they were distilled before experimentation to eliminate peroxide contamination. The concentrations of H_2O_2 were assessed by iodimetric titration (12) and UV spectroscopy (ε_{240} = 39.4 $M^{-1}cm^{-1}$) (13), and that of t-buOOH by iodimetric titration (12). The concentration of alkyl radicals (R•), thermally derived from AAPH (Reaction 1), was calculated using the known rate constant for AAPH decomposition at 37°C, 1.36×10^{-6} s^{-1} (10). Subsequent formation of ROO• (Reaction 2) is diffusion controlled (10).).

Reaction Conditions

Reactions were performed in 500 μL of solutions that were placed in clear 1.5-mL dram vials capped with teflon-lined lids (Kimble Glass, Inc.; Vineland, NJ). Most reactions contained 41.5 μM DHP, 40% (v/v) acetonitrile (ACN), 5 mM phosphate (adjusted to yield the desired pH*; see next section), and various concentrations of the oxidant. Reactions using the above conditions and 1.66 mM H_2O_2 are hereby referred to as "standard reaction conditions." The order of addition was DHP, ACN, water, phosphate and, after a 10-min mixing phase, the oxidant. Peroxide reactions were performed at 40°C and AAPH reactions at 37°C. Stock solutions of DHP, buffer, and oxidant were prepared freshly before experimentation. For some experiments, 100 μM diethyleneaminepentaacetic acid (DTPA) was added, and in other experiments the buffers were treated with Chelex-100, a chelating resin. Values of pH and pH* were determined as described below.

Measurement of pH and pH*

The presence of organic cosolvent affects the measurement of pH with a glass electrode (14). To account for this, aqueous buffer was preadjusted to pH 7.8. After addition of drug and organic cosolvent, the pH* in these mixtures was measured with an Orion 420A pH meter (Orion Research, Inc.; Beverly, MA). The final mixtures contained 41.5 μM DHP, 40% (v/v) organic cosolvent and 5 mM buffer. The pH* values measured in the presence of organic cosolvents were monitored for 2 h and were stable. The magnitude of a cosolvent-dependent pH shift, ΔpH, was determined according to Eq. 1. The ΔpH value for a specific buffer and cosolvent was used to adjust the buffer to the pH that was necessary to yield a specific pH* value. For example, ΔpH for 40% (v/v) ACN was +0.8 for phosphate, +0.1 for [3-*N*-morpholino]propane sulfonic acid (MOPS), and –0.4 for imidazole.

$$\Delta pH = pH^* - pH \qquad \text{(Equation 1)}$$

HPLC Analysis

Reaction mixtures were analyzed on a Luna C-8 5μ column (250 × 4.6 mm id) (Phenomenex; Torrence, CA) using a binary gradient consisting of mobile phase A, 65% methanol (MeOH)/35% formate (50 mM, pH 4), and mobile phase B, 98% MeOH/2% formate, with UV detection at 254 nm. The reverse-phase high-performance liquid chromatography system consisted of two Shimadzu LC-10AS pumps and a Shimadzu SPD-10AV UV/vis detector (Shimadzu; Columbia, MD). Data are reported as the ratio of average peak area of analyte at time × to the average peak area of DHP at time 0 according to Eq. (2).

$$\text{Fraction of analyte} = \langle\text{peak area}\rangle_{t=x}/\langle\text{DHP area}\rangle_{t=0} \qquad \text{(Equation 2)}$$

Spectral Analyses

Ultraviolet (UV) Spectroscopy

UV spectroscopy was used to determine the extent of DHP ionization in various aqueous cosolvent mixtures. The wavelength of maximal absorption, λ_{max}, for DHP was monitored with a Shimadzu UV-160 UV-vis Recording Spectrophotometer. Samples consisted of 33 μM drug in 40% (v/v) ACN or MeOH and 5 mM buffer adjusted to various pH* values (see section "Measurement of pH and pH*"). Plots of λ_{max} vs. pH* were fit to the Boltzman distribution with the Microcal™ Origin™ 5.0 software (Microcal Software, Inc.; Northampton, MA). The fraction of monoionized drug, f_{DH-}, was determined by normalizing λ_{max} to the difference in λ_{max} values for DH_2 and DH^- (255 and 281.5 nm, respectively) using Eq. (3). There was no difference in λ_{max} between DH^- and the fully deprotonated species, D^{2-}.

$$f_{DH-} = \lambda_{max} - \lambda_{max,\,DH_2}/(\lambda_{max,\,DH-} - \lambda_{max,\,DH_2}) \qquad \text{Equation (3)}$$

^{1}H-NMR Sspectroscopy

^{1}H-NMR spectroscopy was used to monitor DHP ionization and the interaction between DHP and buffer. 1-D, HOHAHA, and COSY ^{1}H-NMR experiments were performed on a 500-MHz Bruker Avance spectrometer (Bruker Instruments, Inc.; Billerica, MD). DHP (500 μM) was analyzed in 40% (v/v) ACN-d_3 or MeOH-d_4 and either 5 mM phosphate, MOPS, or imidazole-d_4 in deuterium oxide (D_2O). Reactions were adjusted to the pD* necessary to yield the desired fraction of ionized drug, f_{DH-}. Mixtures of 5 mM buffer and 40% (v/v) ACN-d_3 form concentration gradients, which lead to non-homogeneous magnetic susceptibility and, subsequently, artifactual chemical shifts and splittings. Ultem susceptibility plugs were used to decrease the sample volume and compress the concentration gradient, thus, minimizing non-homogeneity. Interestingly, data acquired in buffer/D_2O containing 40% (v/v) MeOH-d_4 did not encounter the same problems.

Mass Spectrometry

Sample identification was performed by positive FAB-MS on a ZAB HS mass spectrometer (VG Analytical Ltd, Manchester, UK) equipped with a 11/250 data system. FAB-MS experiments were performed using a Xenon gun operated at 8 keV energy and 0.8 mA emission. The sample was dissolved in methylene chloride, dried and placed in a nitrobenzyl alcohol matrix. Matrix and matrix/potassium adduct ions served as bracketing calibrant ions.

Atomic Emission Spectroscopy

Chelex treated buffer samples and controls were submitted for inductively coupled plasma (ICP) optical atomic emis-

sion spectroscopy. Analysis was performed on a Jarrell Ash 975 ICP optical emission spectrometer (Jarrell Ash; Franklin, MA).

RESULTS

Products

The reaction of DHP with peroxides in 40% (v/v) ACN yields three major products, 5,6-dihydro-3(R)-hydroxypyran-2,4-dione (R-OH), 5,6-dihydro-3(S)-hydroxypyran-2,4-dione (S-OH), through hydroxylation at C-3 of the pyrone ring, and a keto-derivative (CO) through oxidative cleavage between the pyrone and the sulfonamide system (for structures, see Fig. 1). The identification of all three products was confirmed by comparison to authentic standards (provided by Pharmacia & Upjohn), where relative retention time and relative response factor are 0.91 and 0.29, respectively, for R-OH, and 0.86 and 0.32, respectively, for S-OH. The identity of CO (molecular weight = 358.4) was confirmed by positive FAB-MS (359.4 m/z, MH^+). Under standard reaction conditions, these products accounted for nearly 100% of the drug lost within the first 30 min of reaction, which is within the first half-life. Therefore, our mechanistic studies focused entirely on the formation of these three products. A representative series of chromatograms, obtained over a 120-min period under standard reaction conditions, is shown in Fig. 1. Importantly, DHP oxidation was significantly more efficient with H_2O_2 than with t-buOOH. This is especially evident from a comparison of the yields of R-OH and S-OH obtained after two hours reaction with 1.66 mM H_2O_2 and 218 mM t-buOOH (Table I).

Although the exposure of DHP to 10 mM AAPH in 40% (v/v) ACN resulted in an ~94% loss of DHP within 2 h, only negligible yields of R-OH, S-OH, and CO formed over the whole time period (data not shown). The majority of the products were not separable from AAPH-related peaks, which eluted near the solvent front, making the product distribution unfit for further study.

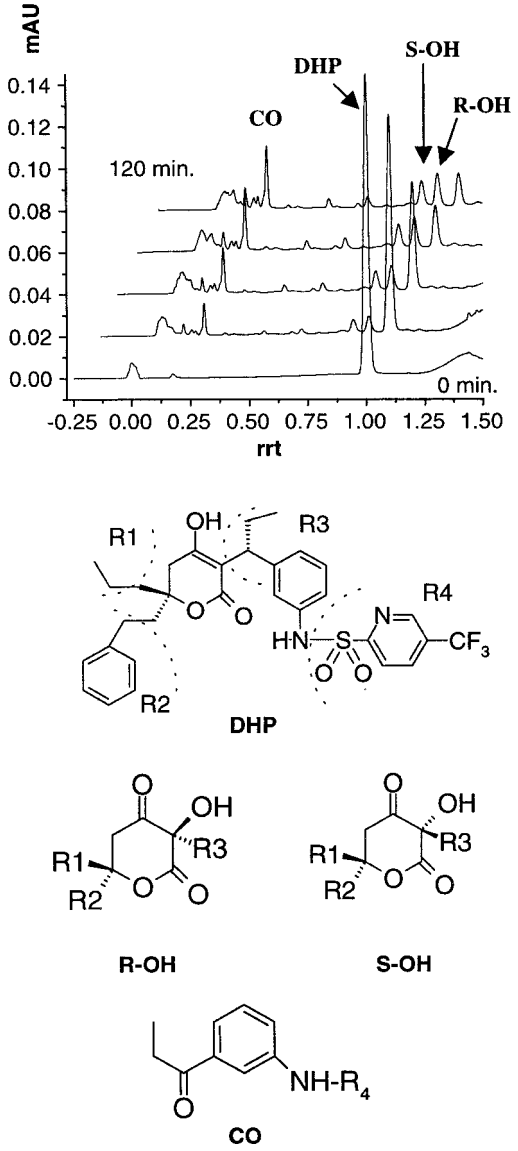

Fig. 1. Upper panel: The chromatographic time course of the reaction between 41.5 μM DHP and 1.66 mM H_2O_2 in 40% (v/v) ACN and 5 mM phosphate (pH* 8.6; f_{DH^-} 1.00) from 0 to 120 min. Lower panel: structures of DHP, R-OH, S-OH, and CO.

Effect of pH*

The deprotonation of the 4-hydroxy group of the pyrone is expected to have a profound influence on the oxidation kinetics of DHP, but the deprotonation of the sulfonamide function will likely be without significant consequences as the sulfonamide function is located remote from the reaction center. Hence, the fractions of DH_2 and DH^- had to be quantified over the pH* region where oxidation was studied. We used UV spectroscopy to monitor the red shift of λ_{max} from 255 nm (DH_2) to 281.5 nm (DH^-). The fraction of DH^-, f_{DH-}, was determined using Equation 3. Titrations were performed in the presence of phosphate, MOPS, and imidazole buffer and fit to Boltzman distributions (Fig. 2). From the sigmoidal fits, we calculated $pK_{a,1}$* in the respective cosolvent systems. (The sigmoidal fits slightly overestimate f_{DH^-} below pH* 7.0 for ACN and 6.2 for MeOH, respectively). The value of $pK_{a,1}$* is 7.2 in 40% (v/v) ACN, which is 1.8 units above the value estimated for aqueous solution (8), and 6.2 in 40% (v/v)

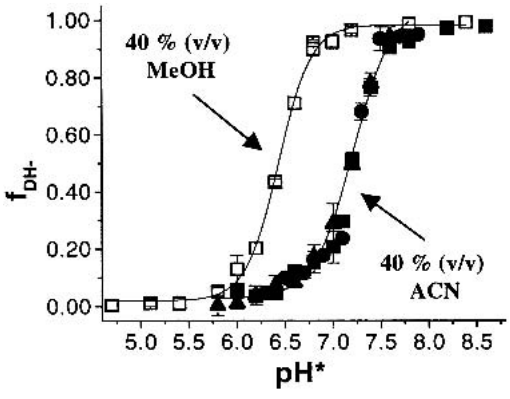

Fig. 2. The ionization of DHP using phosphate (■), MOPS (●), and imidazole (▲) buffers in 40% (v/v) ACN or phosphate buffer in 40% (v/v) MeOH (□) to adjust pH*. Data for each buffer were fit to a Boltzman distribution ($\chi^2 \leq 10^{-3}$) and error bars (SD) may be covered by the symbol.

Table I. Fractions of S-OH, B-OH, and DHP at 2 h for the Reaction of 41.5 μM DHP with Either H_2O_2 or t-buOOH in 5mM Phosphate (pH 8.6) and Various 40% (v/v) Organic Cosolvents

Cosolvent (% (v/v))[a]	Oxidant	S-OH (SD)[b]	R-OH (D)	DHP (SD)
40 ACN	218 mM t-buOOH	0.044 (0.001)	0.062 (0.002)	0.940 (0.025)
40 ACN	1.66 mM H_2O_2	0.191 (0.010)	0.286 (0.013)	0.121 (0.029)
40 MeOH	1.66 mM H_2O_2	0.0	0.0	0.982 (0.039)
38 MeOH/2 ACN	1.66 mM H_2O_2	0.041 (0.003)	0.072 (0.003)	0.851 (0.079)
30 MeOH/10 ACN	1.66 mM H_2O_2	0.119).003)	0.214 (0.005)	0.497 (0.023)
20 MeOH/20 ACN	1.66 mM H_2O_2	0.181 (0.010)	0.300 (0.015)	0.214 (0.014)
70 MeOH/10 BzCN	1.66 mM H_2O_2	0.125 (0.001)	0.221 (0.003)	0.327 (0.003)

[a] The makeup of these solutions to 100% is with water.
[b] SD = standard deviation.

MeOH (titrated only in phosphate buffer). The $pK_{a,1}$* in MeOH is closer to the reported aqueous value, 5.4, because of the water-like, protic nature of MeOH, as opposed to the aprotic nature of ACN (14). The fact that in 40% (v/v) ACN the f_{DH^-} values are independent of the buffer attests to the validity of our method for pH* correction (see section "Measurement of pH and pH*"). Incidentally, titrations performed in mixtures containing 20% (v/v) ACN and 20% (v/v) MeOH, were identical to those in 40% (v/v) MeOH (data not shown).

The oxidation of DHP by 1.66 mM H_2O_2 was performed at pH* 8.6, 7.4, and 6.0 (f_{DH^-} 1.00, 0.65, and 0.07, respectively) in 40% (v/v) ACN containing 5 mM phosphate. In general, the rate of DHP degradation increased with increasing pH*. For pH* = 8.6, drug loss obeyed first order kinetics (Fig. 3A). However, for pH* 7.4 and 6.0 the kinetics of drug loss deviated from first order, suggesting a more complex reaction mechanism. First-order kinetics were also observed for the formation of R-OH and S-OH at pH* 8.6 and 7.4, but not at 6.0 (Fig. 3, B and C). As a result of the larger error limits, we were not able to extract formation kinetics of CO and their dependence on pH* (Fig. 3D).

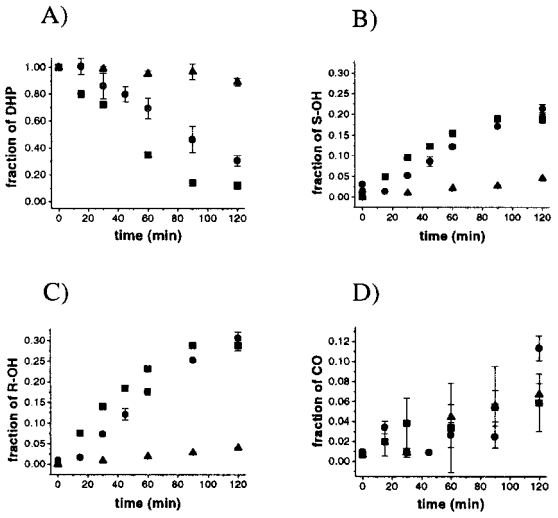

Fig. 3. The kinetic course for the reaction between 41.5 μM DHP and 1.66 mM H_2O_2 in 40% ACN (v/v) and 5 mM phosphate at various pH*: pH* 8.6 (■), 7.4 (●), and 6.0 (▲). (A) Loss of DHP; (B) formation of R-OH; (C) formation of S-OH; and (D) formation of CO. Products are reported as the fraction of initial DHP area, as described by Eq. (2) in the experimental section. Error bars (SD) may be covered by the symbol.

Variation of Buffer

The oxidation of DHP by 1.66 mM H_2O_2 in 40% (v/v) ACN showed identical kinetics in the presence of 5 and 20 mM phosphate buffer, pH* 8.6, indicating that the buffer concentration had no effect on the reaction mechanism. However, there was a remarkable influence of the nature of the buffer on the oxidation kinetics. Under conditions of f_{DH^-} = 1.0 (pH* > 8.0), the rate of DHP loss was fastest in phosphate buffer but significantly slower in MOPS and imidazole, respectively (Fig. 4A). These differences were also reflected in the formation kinetics of R-OH (Fig. 4B; S-OH formation paralleled R-OH formation and data have been omitted). In contrast, meaningful differences in the formation kinetics of CO could not be defined based on the experimental error of the measurement (data not shown). Similar results were observed when reactions in phosphate and imidazole buffer were compared under conditions at f_{DH^-} = 0.76. A potential rationale for the higher stability of DHP in MOPS and imidazole could be ion pairing with the protonated forms of the buffer. This possibility was investigated by ^{1}H-NMR spectroscopy.

^{1}H-NMR Analysis of DHP in the Presence of Buffers

^{1}H-NMR analysis allowed us to compare the chemical shifts of key protons of DHP at various pD* in phosphate, MOPS, and imidazole-d_4. Spectra were collected for 500 μM DHP in 40% (v/v) ACN-d_3 and 5 mM buffer. Proton identities were determined with HOHAHA and key protons have been highlighted in the inset of Figure 5. Assuming that pD* is related to pH* in the same fashion as pD is to pH (pD* = 0.4 + pH*) (15,16) f_{DH^-} was estimated from Figure 2. Incidentally, the spectra collected with 5 mM phosphate (pD* > 8.0) in 40% (v/v) MeOH-d_4 and 40% (v/v) ACN-d_3 closely matched, corroborating that these were spectra of the monodeprotonated form (DH^-) form of DHP.

The C-5 methylene protons of the dihydropyrone, a_1 and a_2 (apparent as a quartet), prove to be sensitive markers for drug ionization and buffer-drug interaction (Fig. 5B). Ionization of the C-4 hydroxyl group shifts a_1 and a_2 upfield. This is evidenced by following the "a" protons from predominantly unionized (i.e., DH_2; bottom two spectra of Fig. 5B) to predominantly ionized DHP (i.e., DH^-; top three spectra in Fig. 5B); however, the magnitude of the upfield shift is less in MOPS and imidazole buffers (0.11 Hz) when compared to phosphate buffer (0.22 Hz). The a_1 proton overlaps with the f protons in spectra for DH_2 (overlap was confirmed with

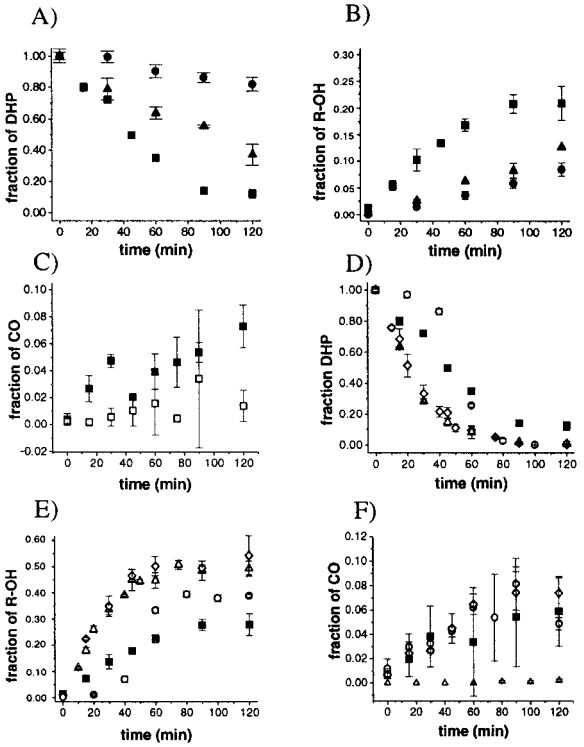

Fig. 4. Kinetic profiles for the loss of DHP and the formation of R-OH and CO with variations of the standard reaction [41.5 μM DHP and 1.66 mM H_2O_2 in 40% (v/v) ACN as well as 5 mM phosphate buffer (pH* 8.6)]. (A and B) The effect of buffer variation on the standard reaction: phosphate (■), MOPS (●), and imidazole (▲). (A) Loss of DHP; (B) formation of R-OH. (C) The effect of performing the standard reaction under atmospheric (■) or N_2-saturated (□) conditions on CO formation. (D–F) Comparison of the standard reaction performed without buffer treatment or metal addition (**Instruction to Composition: insert correct symbol**), with 100 μM DTPA (○), with Chelex treatment (◇) or with 10 μM Cr^{+3} (Δ). (D) Loss of DHP; E) formation of R-OH; and, F) formation of CO. Products are reported as the fraction of initial DHP area, as described by Equation 2 in the experimental section. Error bars (SD) may be covered by the symbol.

COSY); whereas successive ionization to DH^- results in the increasing overlap of a_2 with the f protons, except for $f_{DH^-} = 1.00$ in phosphate. The splitting (Δν) of the "a" protons of DH^- varied between the nitrogen-containing buffers (MOPS and imidazole), $\Delta\nu = 59.4$ Hz, and phosphate, $\Delta\nu = 52.8$ Hz; however, Δν of the "a" protons in DH^- was independent of the buffer, $\Delta\nu = 67.1$ Hz. It should be noted that ^2J, the coupling constant for a_1 and a_2, remained constant under all conditions.

In the aromatic region of the spectra, the o/q doublet, g/k doublet, r singlet and p multiplet experienced decreased resolution with increasing DHP ionization, which becomes evident by following these protons from the bottom (DH_2) to the top spectra (DH^-) in Fig. 5A. The spectra for DH_2 (bottom two spectra in Fig. 5A), shared similar shifts and splittings despite the presence of different buffers (imidazole and phosphate); however, for DH^- (top three spectra in Fig. 5A) all spectra showed buffer-dependent differences.

DH^- specifically showed different spectral characteristics in phosphate compared with MOPS and imidazole buffer. These spectral differences were paralleled by buffer-dependent differences in the oxidation kinetics and would be consistent with drug-buffer ion pairing in MOPS and imidazole, eventually slowing the oxidation.

The Effect of Oxygen

Hydroxylation yields were identical for the standard reaction conditions in oxygenated and N_2-saturated solutions (data not shown), indicating O_2-independent product formation. Conversely, the formation of CO occurred in oxygenated solution but was largely suppressed in N_2-saturated solutions (Fig. 4C), revealing an O_2-dependent production of CO. Hence, the hydroxylation products and CO appear to form via distinctly different reactions.

Hydroxylation as a Function of Cosolvent Nature and Concentration

To assess any cosolvent effect on DHP oxidation, reactions were performed under standard conditions except that the nature and concentration of cosolvent was varied (Table I). In 40% (v/v) ACN, reactions were complete after 2 h, whereas no hydroxylation products were detected in 40% (v/v) MeOH. A similar lack of hydroxylation was noted after two hours in 40% (v/v) acetone, DMSO and 2-propanol, respectively. When ACN was added in small fractions to MeOH, hydroxylation was again observed. Hydroxylation was also accelerated by the addition of benzonitrile to MeOH, indicating a role of the nitrile function in the hydroxylation mechanism. In contrast to hydroxylation, there was no solvent effect on the formation of the carbonyl product, CO, showing similar yields in 40% (v/v) ACN and MeOH.

Effect of Transition Metals

Redox active transition metals can catalyze oxidation and, therefore, any possible involvement of metals in DHP oxidation must be assessed. The addition of 100 μM DTPA to a standard reaction created a 40-min lag phase in the rate of drug loss and hydroxylation (Fig. 4, D and E) and totally inhibited CO formation (Fig. 4F). Independent on the presently unknown rate-determining step, these results suggest that metals may participate in the oxidation mechanisms. A common strategy to minimize transition metal contamination in buffer is the exposure to Chelex-100 mesh resin. However, treatment of the buffers with Chelex did not slow down, but accelerated the degradation of DHP and formation of R-OH and S-OH (Fig. 4, D and E). In contrast, the rate of formation of CO was unaffected by Chelex treatment (Fig. 4F). These data suggest that Chelex treatment of the buffers either led to the contamination of the buffers with a redox-active transition metal or, alternatively, extracted an inhibitory component from the buffers. Surprisingly, the analysis of Chelex-treated buffer by ICP emission spectroscopy did not reveal any significant increase in the concentrations of typical transition metals, such as Co, Cu, Cr, Fe, Mn, Mo, and Ni. Levels of these metals were below the limits of quantitation (i.e., 10 × SD), which ranged from 150 nM for Co to 500 nM for Cr. Addition of 10 nM of these various metals to the standard reaction revealed that none of them was able to accelerate the oxidation of DHP. In fact, Cr^{+3} was the only transition metal which clearly accelerated DHP degradation, albeit at concentrations of 10 μM (Fig. 4, D and E).

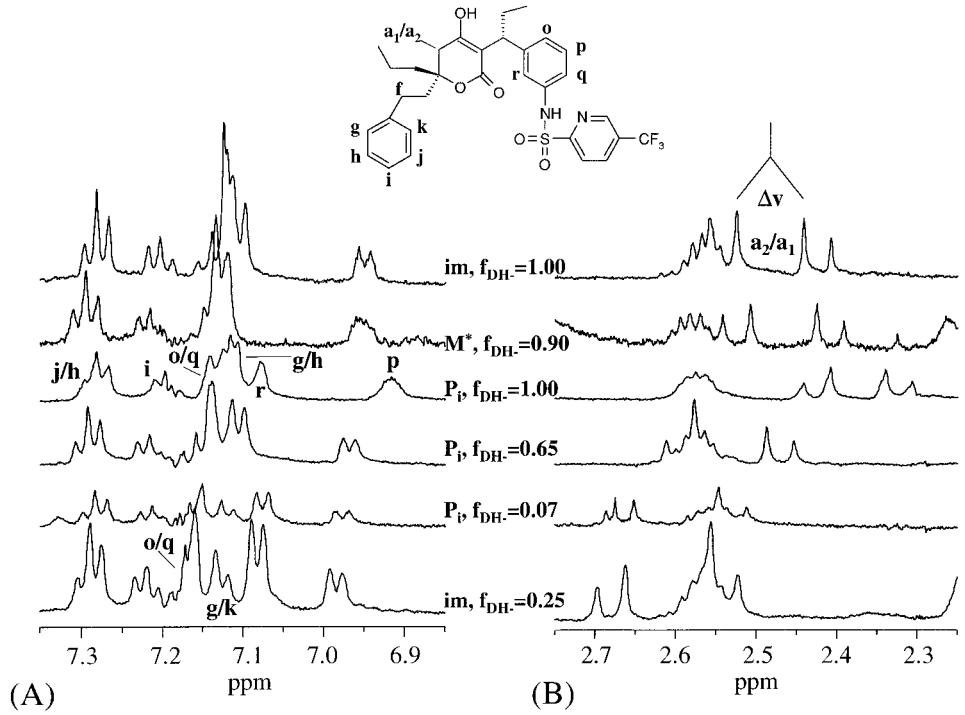

Fig. 5. ^{1}HNMR spectra of 500 μM DHP in 40% (v/v) ACN-d_3 and 5 mM phosphate (P_i), MOPS (M), and imidazole (im) at various pH*. Inset: structure of DHP with key protons labeled. ^{1}HNMR spectral overlay of proton signals in the (A) aromatic and (B) aliphatic regions of spectra. Proton identity was confirmed by HOHAHA ^{1}H-NMR for fully deprotonated DHP in P_i; however, for clarity, the labels for some protons are located in the bottom spectra. *The signal for M has been amplified by a factor of 10.

DISCUSSION

To predict oxidation pathways of DHP in a lipid-based formulation, we used simple binary aqueous-organic cosolvent mixtures with added ROO•, ROOH, and H_2O_2. AAPH-derived ROO• failed to generate a satisfactory product distribution and was not further investigated. The bulk of our mechanistic studies involved standard reaction conditions consisting of 41.5 μM DHP, 1.66 mM H_2O_2, 40% (v/v) ACN, and 5 mM phosphate buffer (pH* 8.6). DHP oxidation with peroxides generated epimeric hydroxylation products, R-OH and S-OH, and a carbonyl-containing product, CO (Fig. 1).

Formation of R-OH and S-OH

The hydroxylation yields and kinetics of DHP in aqueous-organic cosolvent systems by peroxides were governed by the pH*, the nature of the buffer and cosolvent, as well as the presence of metals. At pH* 5.2, where DHP was fully protonated, $f_{DH^-} = 0$, hydroxylation did not occur at measurable rates (Fig. 3, B and C). With increasing pH*, increasing hydroxylation rates were observed. However, for phosphate buffer there was no further acceleration on going from pH* = 7.4 ($f_{DH^-} = 0.65$) to 8.6 ($f_{DH^-} = 1.00$) (Fig. 3, B and C), indicating that deprotonation of DHP may not be the only pH*-dependent parameter affecting DHP hydroxylation. A significant decrease of the hydroxylation rate was observed on going from phosphate to MOPS and imidazole buffers (Fig. 4B). ^{1}H-NMR spectroscopy revealed evidence for ion pair formation between monodeprotonated DHP (DH^-) and MOPS or imidazole (Fig. 5, A and B). Ion pairing between DH^- and a protonated buffer could mask the ionic character of DH^- and/or afford steric protection from oxidant attack. Although the exact conformations for [MOPS-DH^-] and [imidazole-DH^-] are unknown, they likely differ, as evidenced by ^{1}H-NMR spectral differences in the aromatic region (Fig. 5A). DHP hydroxylation proceeded significantly faster in the presence of nitrile-containing cosolvents as compared to MeOH, acetone, DMSO or 2-propanol (Table I). The hydroxylation rates in MeOH were accelerated by the addition of small amounts of ACN, underlining the importance of the nitrile function. These observations can be rationalized by the known tendency of H_2O_2 and organic nitriles (RCN) to form peroxycarboximidic acid, RCH(NH)OOH, under neutral to alkaline conditions (Reaction 3) (17,18).

$$\mathrm{RCN + H_2O_2 \overset{HO^-}{\rightleftharpoons} R{-}C(NH){-}\overset{\delta+}{O}{-}\overset{\delta-}{O}{-}H} \quad (3)$$

$$\mathrm{R{-}C(NH){-}O{-}O{-}H + CH_2{=}CH_2 \longrightarrow R{-}C(O)NH_2 +} \quad (4)$$

This oxidant is extremely unstable and has only recently been identified by FT-Raman and ATR/FTIR spectroscopy (19). Peroxycarboximidic acid is known to epoxidize alkenes (Reaction 4) (17). The ability of peroxycarboximidic acid to transfer an oxygen atom is due to an enhanced electrophilic character of the oxygen distal to the carboximidic moiety, similar to peroxy acids (RC(O)OOH) (20). The oxidation of alkanes by trifluoroperoxyacetic acid (21) and of tertiary amines by peroxycarboximidic acid (22) have recently been reported. The electrophilic oxygen enables nucleophilic attack by electron rich centers such as the double bond in the enolate form (Scheme I; Reactions 5 and 6) or the C3 carbanion in the β-dicarbonylanion of DH^- (Reactions 7 and 8). Both mechanisms would benefit from more alkaline pH by promoting the deprotonation of DHP as well as the formation of the peroxycarboximidic acid. The fact that in phosphate

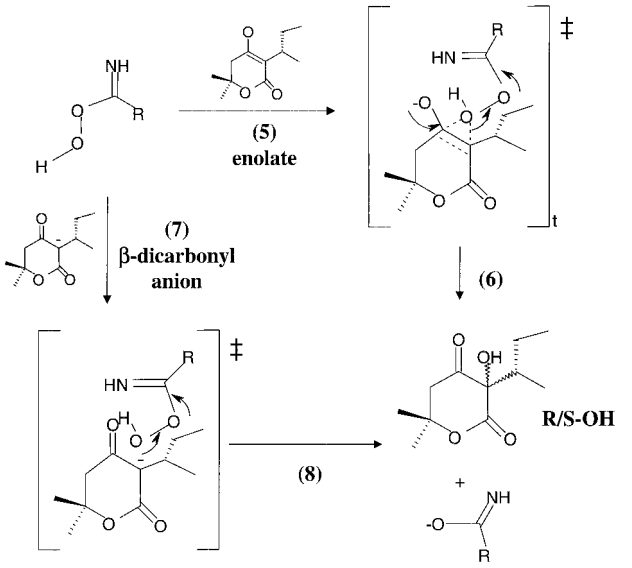

Scheme I.

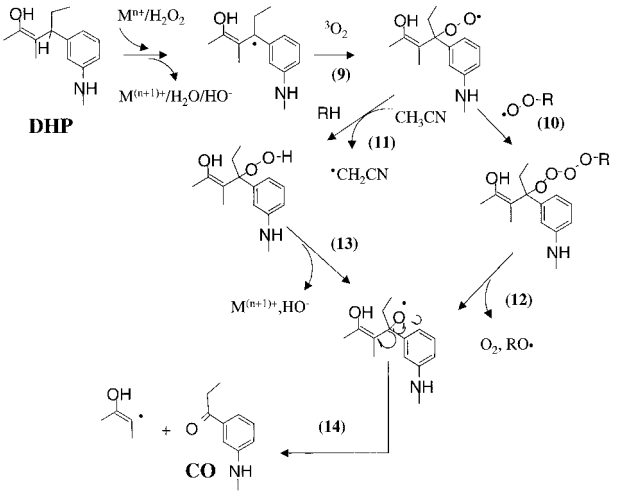

Scheme II.

buffer an increase from pH* 7.4 and 8.6 did not result in further acceleration of hydroxylation may be rationalized by an increased electrostatic repulsion between DH^- and deprotonated peroxycarboximidic acid, $RC(NH)OO^-$. The mechanisms in Scheme I do not account for any dependence of hydroxylation on transition metals (Fig. 4E), suggested by the effect of DTPA. Mechanistically, metals would fit well into the mechanism proposed in Scheme I as it is known that they are able to catalyze epoxidation (24–26) and hydroxylation (26) reactions by peroxides and peroxyacids. However, none of the common redox-active transition metals (Co, Cu, Cr, Fe, Mn, Mo, and Ni) was present even in chelexed phosphate buffer at detectable concentrations. Hence, the nature of the metal remains to be identified. Chelex-treatment either introduces a presently unknown catalytic metal or extracts an inhibitor of DHP oxidation, a possibility that warrants further investigation. In an attempt to identify the catalytic metal(s), we added several of the aforementioned metals to the standard reaction. However, only 10 μM Cr^{+3} enhanced hydroxylation and drug loss to the extent of Chelex treatment (Fig. 4D–E). Even the Fenton reagents (23), Cu^{+2} and Fe^{+3}, did not accelerate hydroxylation.

Formation of CO

Contrary to the mechanism of hydroxylation, the mechanism of carbonyl formation is rather insensitive to pH*, and the nature of the buffer and cosolvent. In fact, only two conditions affected (suppressed) CO formation: N_2-saturation and DTPA addition. These observations can be rationalized by a free radical mechanism, involving hydrogen abstraction at C_1-H of the 3-propyl group in R3 (see Scheme II), followed by the addition of oxygen and classic peroxyl radical chemistry (11) (Scheme II; Reactions 9–14). The reaction of transition metals with peroxides is known to generate reactive oxygen species with hydrogen abstracting capabilities. When complexed to substrate (here, DHP) such metal-bound reactive species will react predominantly with the substrate even in organic solvents (27).

CONCLUSION

During stability testing in water/organic cosolvent mixtures, attention must be given to potential participation of the organic cosolvent in drug degradation. Here, an example is provided for acetonitrile in an oxidative process, and without knowledge of such effects data obtained in binary mixtures may not be representative for lipid-based formulations.

ACKNOWLEDGMENTS

The authors would like to thank Pharmacia for the gift of DHP and financial support of this research. They also thank, at the University of Kansas: Dr. David van der Velde and Dr. Martha Morton for assistance with the ^{1}H-NMR experiments; Mr. Robert Drake for assistance with MS identification; and Mr. Larry M. Magnusson for the ICP emission spectroscopy analysis. Ms. Rachel Andrade of Indiana University assisted Ms. Hovorka during the summer of 2000.

REFERENCES

1. S. Thaisrivongs, P. K. Tomich, K. D. Watenpaugh, K.-T. Chong, W. J. Howe, C.-P. Yang, J. W. Strohbach, S. R. Turner, J. P. McGrath, M. J. Bohanon, J. C. Lynn, A. M. Mulichak, P. A. Spinelli, R. R. Hinshaw, P. J. Pagano, J. B. Moon, M. J. Ruwart, K. F. Wilkinson, B. D. Rush, G. L. Zipp, R. J. Dalga, F. J. Schwende, G. M. Howard, G. E. Padbury, L. N. Toth, Z. Zhao, K. A. Koeplinger, T. J. Kakuk, S. L. Cole, R. M. Zaya, R. C. Piper, and P. Jeffrey. Structure-based design of HIV protease inhibitors: 4-Hydroxycoumarins and 4-hydroxy-2-pyrones as non-peptidic inhibitors. *J. Med. Chem.* **37**:3200–3204 (1994).
2. P. J. Tummino, D. Ferguson, L. Hupe, and D. Hupe. Competitive inhibition of HIV-1 protease by 4-hydroxy-benzopyran-2-ones and by 4-hydroxy-6-phenylpyran-2-ones. *Biochem. Biophys. Res. Commun.* **200**:1658–1664 (1994).
3. P. J. Tummino, D. Ferguson, and D. Hupe. Competitive inhibition of HIV-1 protease by warfarin derivatives. *Biochem. Biophys. Res. Commun.* **201**:290–294 (1994).
4. J. V. N. Vara Prasad, K. S. Para, E. A. Lunney, D. F. Ortwine, Jr., J. Dunbar, D. Ferguson, P. J. Tummino, D. Hupe, B. D. Tait, J. M. Domagala, C. Humblet, T. N. Bhat, B. Liu, D. M. A. Guerin, E. T. Baldwin, J. W. Erickson, and T. K. Sawyer. Novel series of achiral, low molecular weight, and potent HIV-1 protease inhibitors. *J. Am. Chem. Soc.* **116**:6989–6990 (1994).
5. S. Thaisrivongs, H. I. Skulnick, S. R. Turner, J. W. Strohbach, R. A. Tommasi, P. D. Johnson, P. A. Aristoff, T. M. Judge, R. B. Gammill, J. K. Morris, K. R. Romines, R. A. Chrusciel, R. R.

Hinshaw, K.-T. Chong, G. W. Tarpley, S. M. Poppe, D. E. Slade, J. C. Lynn, M.-M. Horng, P. K. Tomich, E. P. Seest, L. A. Dolak, W. J. Howe, G. M. Howard, F. J. Schwende, L. N. Toth, G. E. Padbury, G. J. Wilson, L. Shiou, G. L. Zipp, K. F. Wilkinson, B. D. Rush, M. J. Ruwart, K. A. Koeplinger, Z. Zhao, S. L. Cole, R. M. Zaya, T. J. Kakuk, M. N. Janakiraman, and K. D. Watenpaugh. Structure-based design of HIV protease inhibitors: Sulfonamide-containing 5,6-dihydro-4-hydroxy-2-pyrones as nonpeptidic inhibitors. *J. Med. Chem.* **39**:4349–4353 (1996).

6. S. Thaisrivongs, D. L. Romero, R. A. Tommasi, M. N. Janakiraman, J. W. Strohbach, S. R. Turner, C. Biles, R. R. Morge, P. D. Johnson, P. A. Aristoff, P. K. Tomich, J. C. Lynn, M.-M. Horng, K.-T. Chong, R. R. Hinshaw, W. J. Howe, B. C. Finzel, and K. D. Watenpaugh. Structure-based design of HIV protease inhibitors: 5,6-Dihydro-4-hydroxy-2-pyrones as effective, nonpeptidic inhibitors. *J. Med. Chem.* **39**:4630–4642 (1996).
7. M. N. Janakiraman, K. D. Watenpaugh, P. K. Tomich, K.-T. Chong, S. R. Turner, R. A. Tommasi, S. Thaisrivongs, and J. W. Strohbach. Non-peptidic HIV protease inhibitors: C_2-Symmetry-based design of bis-sulfonamide dihydropyrones. *Bioorg. Med. Chem. Lett.* **8**:1237–1242 (1998).
8. G. E. Padbury, G. L. Zipp, F. J. Schwende, Z. Zhao, K. A. Koeplinger, K.-T. Chong, T. J. Raub, and S. Thaisrivongs. Factors impacting the delivery of therapeutic levels of pyrone-based HIV protease inhibitors. In R. T. Borchardt, R. M. Freidinger, T. K. Sawyer, and P. L. Smith (eds.), *Integration of Pharmaceutical Discovery and Development: Case Studies*, edition, Plenum Press, New York, 1998 pp. 211–232.
9. N. A. Porter. Mechanisms for autoxidation of polyunsaturated lipids. *Accounts Chem. Res.* **19**:262–268 (1986).
10. E. Niki. Free radical initiators as source of water- or -lipid-soluble peroxyl radicals. *Methods Enzymol.* **186**:100–108 (1990).
11. C. von Sonntag and H.-P. Schuchmann. Peroxyl radicals in aqueous solutions. In Z. B. Alfassi (ed.), *Peroxyl Radicals*, John Wiley & Sons, New York, 1997 pp. 173–234.
12. D. C. Harris. *Quantitative Chemical Analysis*, Chapter 16. Redox Titrations, 4th edition, W.H. Freeman and Company, New York, 1995.
13. D. P. Nelson and L. A. Kiesow. Enthalpy of decomposition of hydrogen peroxide by catalase at 25°C. *Anal. Biochem.* **49**:474–478 (1972).
14. R. G. Bates. Medium effects and pH in nonaqueous solvents. In C. D. Ritchie, and J. F. Coetzee (eds.), *Solute-Solvent Interactions*, Marcel Dekker, Inc., New York, 1969 pp. 45–96.
15. P. K. Glasoe and F. A. Long. Use of glass electrodes to measure acidities in deuterium oxide. *J. Phys. Chem. A* **64**:188–191 (1960).
16. K. B. J. Schowen. Solvent hydrogen isotope effects. In R. D. Gandour, and R. L. Schowen (eds.), *Transition-States of Biochemical Processes*, Plenum Press, New York, 1978 pp. 225–283.
17. G. B. Payne, P. H. Deming, and P. H. Williams. Reactions of hydrogen peroxide. VII. Alkali-catalyzed epoxidation and oxidation using a nitrile as a co-reactant. *J. Org. Chem.* **26**:659–663 (1961).
18. Y. Sawaki and Y. Ogata. Mechanism of the reaction of nitriles with alkaline hydrogen peroxide. Reactivity of peroxycarboximidic acid and application to superoxide ion reaction. *Bull. Chem. Soc. Japan* **54**:793–799 (1981).
19. V. Vacque, N. Dupuy, J. P. H. Sombret, and P. Legrand. In situ characterisation of peroxycarboximidic acid by FT-raman and ATR/FTIR spectroscopy. *J. Mol. Structure* **384**:165–174 (1996).
20. B. Plesnicar. Polar reaction mechanisms involving peroxides in solution. In S. Patai (ed.), *The Chemistry of Peroxides*, John Wiley & Sons, New York, 1983 pp. 521–584.
21. D. M. Camaioni, J. T. Bays, S. J. Shaw, J. C. Linehan, and J. C. Birnbaum. Radical and non-radical mechanisms for alkane oxidation by hydrogen peroxide-trifluoroacetic acid. *J. Org. Chem.* **66**:789–795 (2001).
22. G. Laus. Kinetics of acetonitrile-assisted oxidation of tertiary amines by hydrogen peroxide. *J. Chem. Soc. Perkin Trans.* **2**:864–868 (2001).
23. S. Goldstein, D. Meyerstein, and G. Czapski. The Fenton reagents. *Free Radic. Biol. Med.* **15**:435–445 (1993).
24. H. Mimoun. Transition-metal peroxides—synthesis and uses as oxidizing agents. In S. Patai (ed.), *The Chemistry of Peroxides*, John Wiley & Sons, New York, 1983 pp. 463–482.
25. D. V. Deubel, J. Sundermeyer, and G. Frenking. Mechanism of the olefin epoxidation catalyzed by molybdenum diperoxo complexes: Quantum chemical calculations give an answer to a long-standing question. *J. Am. Chem. Soc.* **122**:10101–10108 (2000).
26. M. Torrent, M. Solá, and G. Frenking. Theoretical studies of some transition-metal-mediated reactions of industrial and synthetic uses. *Chem. Rev.* **100**:439–493 (2000).
27. D. T. Sawyer, A. Sobkowiak, and T. Matsushita. Metal [MLx; M = Fe, Cu, Co, Mn]/hydroperoxide-induced activation of dioxygen for the oxygenation of hydrocarbons: Oxygenated Fenton chemistry. *Accounts Chem. Res.* **29**:409–416 (1996).